ADVANCED MATERIALS
www.advmat.de

Optical Fibers Embedded with As-Grown Carbon Nanotubes for Ultrahigh Nonlinear Optical Responses

Qi Xiao, Jin Xie, Guangjie Yao, Kaifeng Lin, Hao-Li Zhang, Liu Qian,* Kaihui Liu,* and Jin Zhang**

Photonic crystal fiber (PCF) embedded with functional materials has demonstrated diverse applications ranging from ultrafast lasers, optical communication to chemical sensors. Many efforts have been made to fabricating carbon nanotube (CNT) based optical fibers by ex situ transfer method; however, often suffer poor uniformity and coverage. Here, the direct growth of CNTs on the inner walls of PCFs by the chemical vapor deposition (CVD) method is reported. A two-step growth method is developed to control the narrow diameter distribution of CNTs to ensure desirable nanotube optical transitions. In the as-fabricated CNT- embedded fiber, third-harmonic generation (THG) has been enhanced by ≈15 times compared with flat CNT film on fused silica. A dual-wavelength all-fiber mode-locked ultrafast laser (≈1561 and ≈1064 nm) is further demonstrated by integrating the 1.36±0.15 nm-diameter CNTs into two kinds of photonic bandgap hollow core PCF (named HC-1550 and HC-1060) as saturable absorbers, using their S_{11} (≈0.7 eV) and S_{22} (≈1.2 eV) interband transition respectively. The fiber laser shows stable output of ≈10 mW, ≈800 fs pulse width, and ≈71 MHz repetition rate at 1561 nm wavelength. These results can enable the large-scale applications of CNTs in PCF-based optical devices.

1. Results and Discussion

Carbon nanotube (CNT) is a promising material in photonic and nonlinear optical applications due to its excellent properties of sub-picosecond recovery time, broadband response (0–2 eV), low saturation intensity (only one-twentieth of that of graphene), as well as perfect single-crystalline structure.[1] By embedding CNTs into an optical fiber, the light-CNT interaction length can be greatly enhanced through evanescent wave couplings, providing even more opportunities for their use. Additionally, the 1D structure of CNTs, which forms an ultrathin film, will not interfere with the transmission mode of optical fibers.

Previous efforts have focused on transferring CNTs[2] onto side-polished,[3] tapered normal optical fibers,[4] or filling them into the holes of hollow capillary fibers (HCFs).[5] However, the ultralarge aspect ratio of CNTs makes them prone to binding with each other. When CNT bundles are forced open with the assistance of surfactants and violent forces, the integrity of CNT structures may be compromised and introduce impurities that are hard to eliminate, hindering the reliable and large-scale transfer of high-quality CNTs. Additionally, treatments necessary to enable CNTs interact with light propagation in normal optical fibers has undesirable effects on the hybrid fiber. For example, side-polished fiber leads to unwanted polarization dependence,[6] tapered fiber causes large insertion loss and alters the fundamental transmission mode,[7] and HCF causes large coupling loss when connected to single-mode systems.[5]

Q. Xiao, J. Zhang
Beijing Science and Engineering Center for Nanocarbons
School of Materials Science and Engineering
College of Chemistry and Molecular Engineering
Peking University
Beijing 100871, P. R. China
E-mail: jinzhang@pku.edu.cn

Q. Xiao, H.-L. Zhang
State Key Laboratory of Applied Organic Chemistry
Key Laboratory of Special Function Materials and Structure Design
College of Chemistry and Chemical Engineering
Lanzhou University
Lanzhou 730000, P. R. China
E-mail: haoli.zhang@lzu.edu.cn

J. Xie, G. Yao, K. Lin, K. Liu
State Key Laboratory for Mesoscopic Physics
Academy for Advanced Interdisciplinary Studies
School of Physics
Peking University
Beijing 100871, P. R. China
E-mail: khliu@pku.edu.cn

L. Qian, J. Zhang
School of Materials Science and Engineering
Peking University
Beijing 100871, P. R. China
E-mail: qianliu-cnc@pku.edu.cn

The ORCID identification number(s) for the author(s) of this article can be found under https://doi.org/10.1002/adma.202303046

DOI: 10.1002/adma.202303046

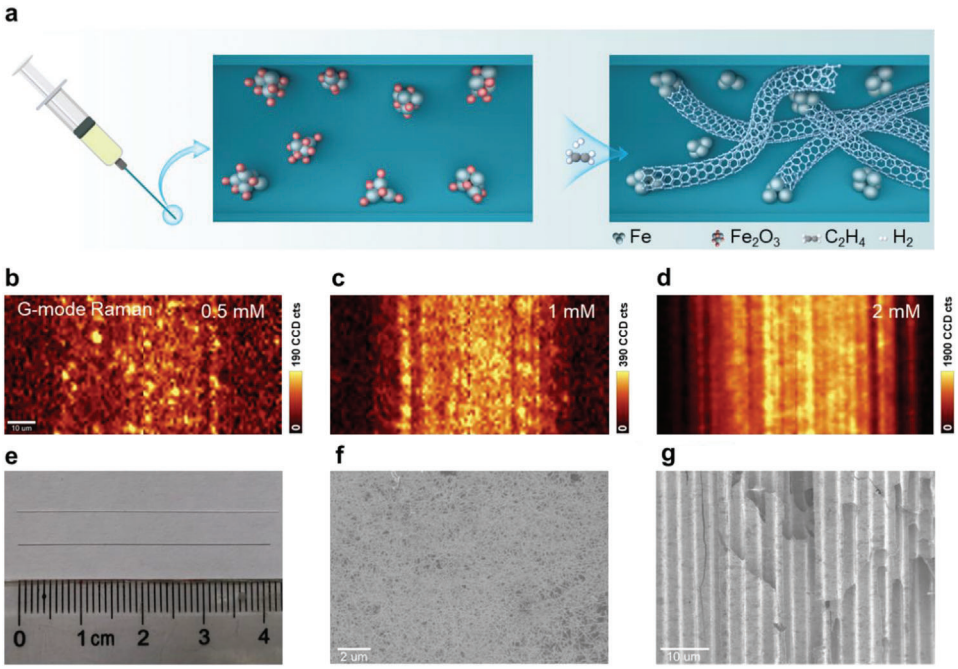

Figure 1. Growth of a high-density, uniform CNT-embedded optical fiber. a) Schematic of the growth method, consisting of the injection of $FeCl_3$ into fiber holes and drying at a moderate speed followed by high-temperature growth. b–d) G-mode Raman mapping of CNT-PCF, showing the dependence of CNT density on the $FeCl_3$ catalyst precursor concentrations of 0.5 mmol L^{-1} (b), 1 mmol L^{-1} (c), and 2 mmol L^{-1} (d), respectively. e) Optical image of bare PCF and CNT-PCF. f,g) Typical SEM image of the fractured CNT-PCF, showing full coverage, randomly oriented CNT "fabric" uniformly grown on the inner wall.

Currently, as the development of photonic crystal fibers (PCFs),[8,9] whose porous structures provide spaces for material growth, 2D materials such as graphene and MoS_2 have been successfully grown on the inner walls of the fiber. The centimeters-long graphene-PCF and MoS_2-PCF showed strong light–matter interactions and enhanced nonlinearity.[8c,d,10] In contrast to graphene without a bandgap or MoS_2 with a certain large bandgap, CNTs exhibit a broadband response (0–2 eV) and exquisite interband structures, benefiting broadband operation in optical and nonlinear optics.[2b,11] However, growing CNTs is more challenging due to the need for extra diameter control, which greatly influences their bandgaps. For nonlinear optical applications involving CNTs embedded in optical waveguide, only the CNT segment resonating with the operating wavelength contributes positively, while the rest of CNTs induce detrimental effects such as extra absorption and scattering loss.[2a] Unfortunately, traditional CNT-based optical fiber fabrication methods rarely achieve diameter control of CNTs, and full coverage of CNT film is required for sufficient interaction area due to the weak evanescent light. Therefore, an efficient and undamaged fabrication strategy for producing high-coverage CNT optical fiber complexes with large-scale uniformity is crucial for real applications.

Here, we report the successful direct growth of full-coverage CNTs on the inner wall of a PCF using the chemical vapor deposition (CVD) method. This achievement builds on previous experiences in growing CNT horizontal arrays with controlled structures[12] and high density.[13] Our growth strategy consists of two steps, as illustrated in **Figure 1**a. First, Fe catalyst precursors were filled into the fiber holes via injection of $FeCl_3$ ethanol solution (Figure 1a, left). Next, the fiber was moved into a CVD furnace and dried for 2 h at a low temperature of 200 °C, where the Fe precursors were gradually oxidized and coated onto the inner fiber walls (Figure 1a, middle). The furnace temperature was then raised to ≈820 °C, and 200 standards cubic centimeters per minute (sccm) of H_2 were introduced to reduce the catalyst precursors to Fe catalyst nanoparticles. Finally, after the introduction of a carbon source (ethylene, 50 sccm), the CNTs grew along the inner wall of the fiber (Figure 1a, right). The entire growth process was carried out under low-pressure conditions, where the gas flow was able to overcome the large viscous force within the micrometer-sized hole walls,[8c] resulting in homogeneous CNT growth.

In our growth method, the CNT coverage can be easily adjusted by varying the concentration of the $FeCl_3$ solution. By increasing the solute concentration from 0.5 to 1 to 2 mmol L^{-1}, we observed a gradual increase in CNT coverage, from sporadic dispersion (Figure 1b) to moderate distribution (Figure 1c) to full coverage (Figure 1d), as reflected by G-mode Raman mappings of the CNT-PCFs. The increase in coverage was also confirmed by the increased contrast of the CNT-PCF photographs and more directly by the increased density of CNTs in the scanning electron microscopy (SEM) images of the CNT-PCF fracture surface (Figure S1, Supporting Information). A further increase in the $FeCl_3$ concentration resulted in poor quality of CNTs, as indicated by a high-intensity ratio of D- to G-mode in the Raman spectrum (Figure S2, Supporting Information).

Under our optimized conditions, we successfully achieved homogeneous CNT growth on the hole walls of a 4-cm-long optical fiber (Figure 1e; Figure S3, Supporting Information). We also broke the CNT-PCF to directly visualize the CNT dispersion

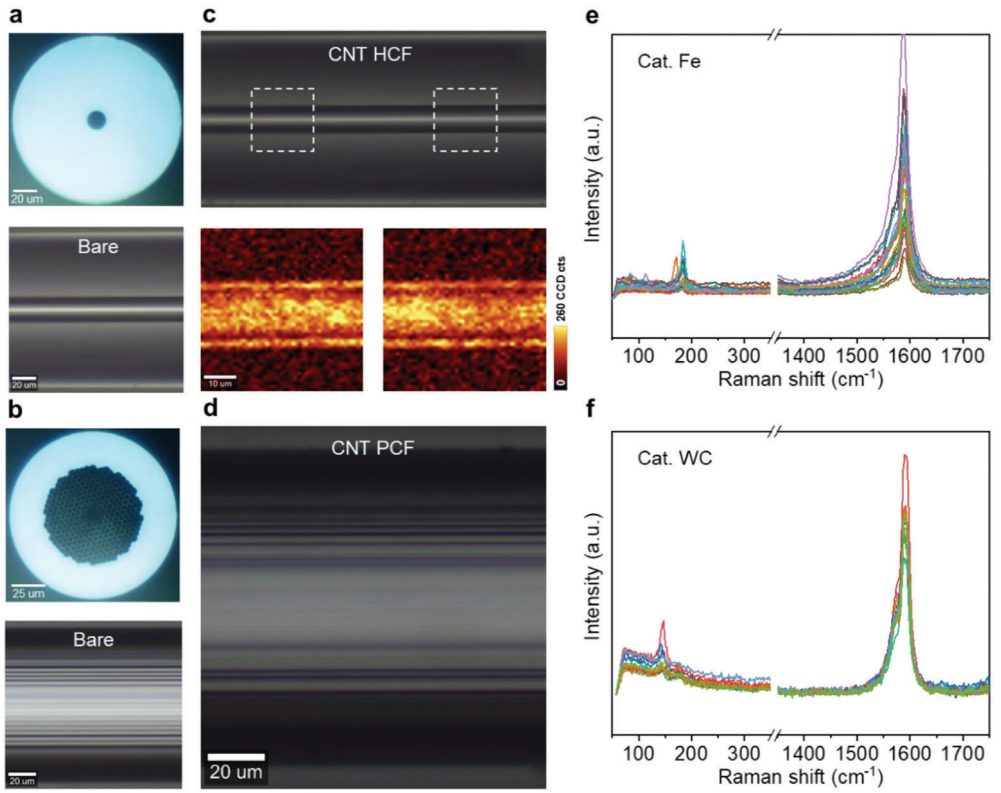

Figure 2. CNT-embedded optical fibers with diverse fiber structures and well-controlled diameters. a,b) Top (top) and side (bottom) views of an HCF with a core diameter of ≈15 µm (a) and a PCF (HC-1550) with a hollow-core honeycomb structure (b). c,d) Side view of HCF and PCF after the growth of CNT, showing slightly higher contrast compared with the bare ones (a,b). The bottom of (c) is the G-mode Raman intensity mapping in white dash square, showing the full coverage of CNT in the inner wall. e,f) Raman spectra of the CNT-PCF grown by Fe and WC catalyst, using line mapping along the radial direction with scan step of 3 µm and an excitation laser of 633 nm, indicating well-controlled diameters.

(Figure S4c,d, Supporting Information). The inner wall of the fiber exhibited long CNTs interlaced with each other, forming a perfect CNT film, like a "fabric" (Figure 1f), which was uniformly dispersed in all the hole walls (Figure 1g; Figure S4c,d, Supporting Information). This randomly oriented CNT "fabric" on the inner wall of optical fibers brings additional advantages of polarization independence when used in photonics or nonlinear optics. We also conducted a controlled experiment, where we filled the fibers with catalyst precursor $FeCl_3$ through capillary filling instead of injection (as performed in MoS_2-PCF growth). We found that only a few CNTs sporadically distributed in the fiber, and the coverage of CNT could not be increased by changing the concentration of $FeCl_3$ solution or any other growth conditions using this strategy (Figure S5, Supporting Information). Therefore, the injection of Fe catalyst precursors into the fiber holes is the crucial step for achieving full coverage growth of uniform CNT films onto the fibers.

Our growth method for the CNT-embedded optical fiber has been proven to be versatile, and applicable to different fiber structures (**Figure 2**a,b) and narrow diameter distributions. In addition to CNT-PCFs (Figure 2b,d), we have successfully achieved homogeneous CNT growth in HCFs with various hole diameters (ranging from 50 to 15 to 5 µm), as shown in Figure 2a,c and Figure S4a–d in the Supporting Information. As the diameter of the fiber hole decreases, gas flow in the narrower space experiences greater viscous force,[8c] requiring lower pressure and a higher carbon-hydrogen ratio for CNT growth.

Our growth method has also enabled the fabrication of CNT fibers with different diameter distributions by altering the types of catalyst precursor solutions. According to the CNT growth mechanism,[12a] the size uniformity of the catalyst nanoparticles is a crucial factor for controlling the CNT diameter. For example, large Fe metal catalyst particles with high vapor pressure will rapidly vaporize under low-pressure and high-temperature conditions, leaving behind smaller nanoparticles. Under optimized growth conditions, we obtained CNTs with small diameters of 1.36±0.15 nm, as calculated from RBM peak positions in Raman line mapping (Figure 2e; Figure S6a, Supporting Information).[14] Notably, Raman line mapping measurements were taken along the radial direction with a scan step of 3 µm, as the small hole of PCF is ≈3 µm, to avoid the possibility of testing the same CNT due to random orientations. The variation of Raman intensities is due to the mismatch of polarizations between the randomly oriented CNT film and the excitation laser, as well as the position fluctuation of the laser focus on the photonic crystal surface. However, the fluctuations do not influence the Raman shifts in the spectra. Conversely, using $(NH_4)_6W_7O_{24}$ as the catalyst precursor results in the formation of a WC catalyst, which catalyzes CNT growth under the same conditions.[12a] This leads to larger CNT diameters of 1.69±0.10 nm (Figure 2f;

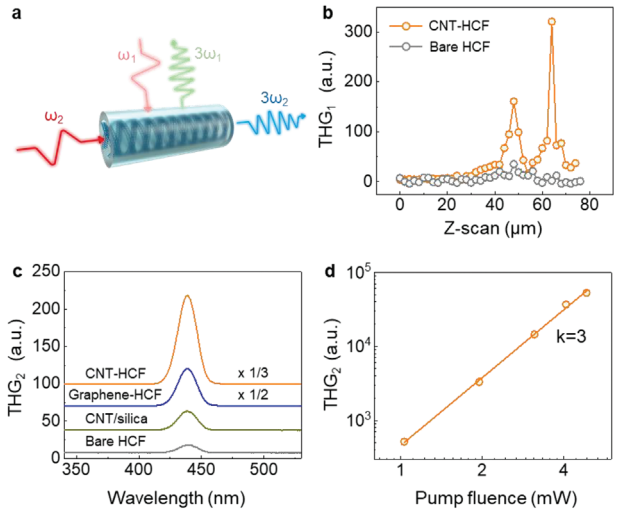

Figure 3. CNT-embedded optical fibers with harmonic enhancement. a) The schematic diagram of THG in CNT-HCF. b) The THG intensity varies with the depth of the incident laser ω_1 focused on the fiber sidewall. c) The THG spectra excited by the laser ω_2 along the fiber direction (CNT-HCF, graphene-HCF, CNT/silica, and bare HCF) at the same incident power (≈5 mW) and the same length (≈3 cm). The peak intensity ratio of the four samples is about 33:9:2:1. d) Dependence of the THG signal intensity of the CNT-HCF on the incident optical power.

Figure S6b, Supporting Information), as relatively large WC catalyst nanoparticles remain due to their high melting point and low vapor pressure. As a typical solid catalyst at growth temperature, the as-grown CNTs exhibit narrower diameter distributions than liquid catalyst Fe.

Direct measurement of the particle size of these catalysts is challenging due to the high curvature of the fiber's inner wall. Thus, we utilized a spatially confined CVD method to monitor the CNT growth conditions in an optical fiber. By using quartz-Si/SiO_2 stacking with a cubic weight on the quartz, a gap of <10 μm was formed,[15] similar to PCF hole diameter, allowing for gas flow monitoring (Figure S7, Supporting Information). We maintained the temperature and pressure of the furnace identical to those used for CNT-PCF growth and determined the size of catalyst nanoparticles by AFM. The average diameter of Fe nanoparticles was ≈2.0 nm (Figure S7b,d, Supporting Information), smaller than that of tungsten-based nanoparticles (≈2.4 nm, Figure S7c,e, Supporting Information), consistent with our former analysis. The as-grown CNT-embedded optical fibers are well-suited for nonlinear optical applications.

Conventional silica-based optical fibers have limited applications in nonlinear optics, such as frequency conversion, nonlinear harmonic generation, and supercontinuum generation, due to the small real part of the third-order nonlinear susceptibility ($n_2 \approx 3 \times 10^{-16}$ cm^2 W^{-1})of fused-silica materials. However, by embedding CNTs into the fused-silica optical fiber, the third-harmonic generation (THG) signal can be enhanced, as the evanescent wave interacts with the CNT film along the fiber direction (**Figure 3**a). The nonlinear polarization of π-electrons in the carbon honeycomb network gives CNTs ultrahigh third-order nonlinearity ($n_2 \approx 3 \times 10^{-8}$ cm^2 W^{-1}), which can be enhanced by excitons in the 1D structure.[16] Here, we used HCFs for CNT film growth and THG measurement due to their broader transmission window than photonic bandgap PCFs (Figure S8, Supporting Information), which allows both pump pulses and THG signals to propagate. To characterize the HCFs covered by CNT film, a femtosecond pulse (ω_1) is vertically incident to the side wall of the HCF to measure its THG intensity. Upon introducing CNTs into the HCF, two distinct peak THG intensities separated by 15 μm appear, corresponding to the HCF's internal diameter of 15 μm (Figure 3b). The transmittance of HCFs embedded with different CNT diameter distributions is also measured (Figure S8, Supporting Information). The CNT-HCF with a tube diameter of ≈1.36 nm exhibited low transmittance near 1500 nm, which corresponds to its S_{11} absorption peak.

THG enhancement performance of HCFs with different CNTs coverage and fiber length excited by the laser (ω_2) along the fiber direction were measured. Nevertheless, a trade-off exists between the harmonic enhancement effect and the linear absorption loss, as both the excitation light and the THG signal overlap with the CNT's absorption. The harmonic enhancement reached its maximum value in the full coverage sample with the fiber length of 3 cm, which displayed a ≈30-fold increase of THG signals compared to that of bare HCF (Figure 3a; Figure S9, Supporting Information). Such CNT-HCF exhibited a ≈15 fold higher THG signal strength than the flat CNT film on fused silica (Figure 3c) and even higher than that of monolayer graphene-HCF (Graphene-HCF is grown using our previous approach,[8c,10a] detailed characterization shown in Figure S10 in the Supporting Information). The cubic relationship between the intensity of the THG signal and the incident optical power is consistent with theoretical expectations (Figure 3d). The THG signal can be further enhanced by several orders of magnitude if the phase matching between the THG and the fundamental frequency light is satisfied by extra fiber structure design.[8d,17]

The nonlinear absorption properties of CNTs are determined by the imaginary part of the refractive index, which endows them with saturable absorption properties for laser mode-locking.[18] Here, we prepared semiconductor CNTs with an average tube diameter of ≈1.36 nm, which exhibited first and second interband transition energies (S_{11} and S_{22}) at ≈0.7 and 1.2 eV, corresponding to two common near-infrared bands (≈1550 and ≈1060 nm, **Figure 4**a). To ensure mode-matching, two photonic bandgap PCFs operating at 1550 and 1060 nm respectively (named HC-1550 and HC-1060) are employed as substrates for the growth of CNTs, each with a length of 3 cm. The as-fabricated CNTs-HC-1550 and CNTs-HC-1060 samples were excited by femtosecond pulsed lasers at 1550 and 1064 nm, respectively. The corresponding modulation depths and saturation absorption intensities are 6.5%/4.1% and 7.6/14.4 MW cm^{-2}, respectively (Figure 4b). The saturation absorption intensity of S_{22} was approximately twice that of S_{11}, mainly due to the faster inter-subband transition in which the relaxation process from S_{22} to S_{11} dominates.[19] In general, most mode-locked fiber lasers opt for the S_{11} of the CNTs, corresponding to a single real gap in electron density of states, because S_{11} facilitates self-start mode-locking at low pump power. Whereas, the shorter lifetime of S_{22} may also have positive significance for mode-locking and enable the extension of the operating band to visible operating bands below 1μm.[20]

The CNT film embedded HC-1550 and HC-1060 are employed as mode-locking elements for two ring-cavity fiber lasers

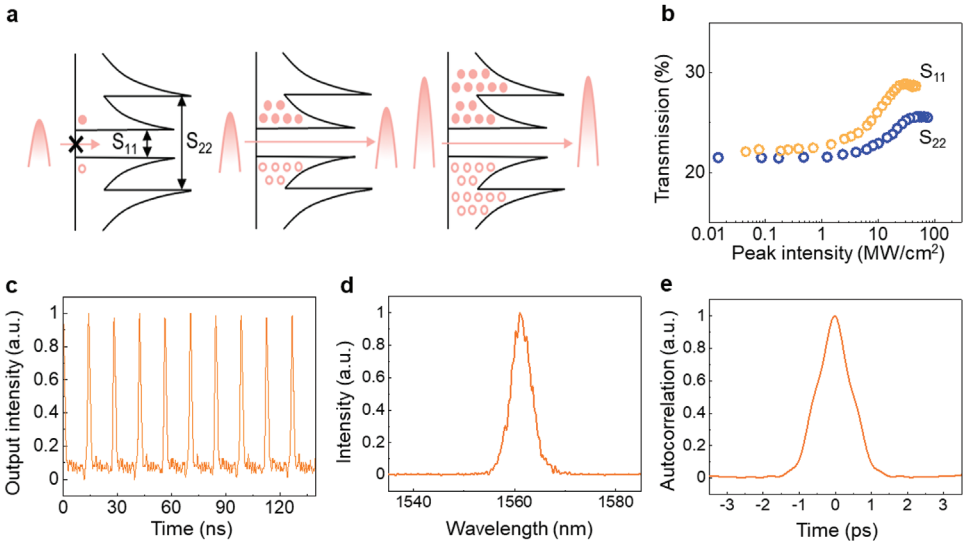

Figure 4. Stretched soliton generated by CNT-embedded HC-1550-based mode-locked ring fiber lasers. a) Schematic diagram of saturable absorption of CNTs corresponding to the S_{11} and S_{22} absorption edges respectively. b) Saturable absorption measurement of CNTs with a diameter of 1.36 nm embedded in fibers (blue for HC-1060 and orange for HC-1550), with modulation depths of 4.1% and 6.5%, respectively. c–e) Output results from a ring-cavity fiber laser with an average tube diameter of 1.36±0.15 nm CNTs embedded in HC-1550 fiber as a SA, where (c) is a pulse train with ≈14 ns interval (≈71 MHz), (d) is output spectrum with a central wavelength at 1561 nm and (e) is an autocorrelation trace with FWHM of ≈800 fs.

using erbium-doped and ytterbium-doped fiber gain media, respectively, and operating at wavelengths of 1064 and 1561 nm. For the mode-locked Er-doped fiber laser, the total group velocity dispersion (GVD) is designed to be 0.001 ps^2 by dispersion management. The laser was pumped by a 980 nm laser diode and coupled into a ring cavity by a 980/1550 nm wavelength division multiplexer. A polarization controller (PC) and a polarization-independent isolator were employed to control the birefringence and the unidirectional pulse propagation within the cavity (Figure S11a, Supporting Information). By carefully adjusting the PC, a 1.23 ps stretched pulse with a central wavelength of 1561 nm is generated at a pump power of 300 mW (Figure 4d; Figure S11b, Supporting Information). The repetition frequency of the output laser is 71 MHz, corresponding to the total cavity length. The pulse width could be further compressed to ≈800 fs using out-of-cavity dispersion compensation based on the time-bandwidth limit theory, given the spectral width of 4.7 nm (Figure 4c,e). The maximum average output power is about 10.0 mW, corresponding to the single pulse energy of about ≈140 pJ. Typically, ultrafast fiber lasers that use nonlinear low-dimensional materials embedded into the air holes of PCF as saturation absorbers exhibit ease of integration and superior damage threshold power compared to the film directly attached to the fiber end face. For instance, all fiber lasers based on MoS_2-PCF produce a pulse width of ≈500 fs operating at 1550 nm, while graphene-PCF produces a pulse width of ≈2 ps.[8d,10a] In our design, by adjusting the diameter of CNTs and selecting the PCF of a specific working wavelength, we can flexibly tune the laser's operating wavelength and generate sub-1 ps laser pulses, highlighting the superiority of our CNT-PCFs.

We also designed a fiber ring cavity operating at 1064 nm, consisting of a 0.65 m highly ytterbium-doped fiber (YDF, LIEKKI Yb1200-4/125) and a 2.85 m single-mode fiber (HI 1064) (Figure S12a, Supporting Information). The net cavity dispersion is normal, with an estimated value of 0.0782 ps^2. The intracavity mode-locking component consisted of the same diameter CNTs used in the 1561 nm fiber laser described above. However, the operating wavelength of the laser, in this case, corresponds roughly to the S_{22} absorption edge, and the CNTs are embedded in HC-1060 at an operating band of around 1060 nm. Since the S_{22} utilized here requires larger pump energy to reach saturation, we obtain the bound soliton state at the fundamental repetition rate at the pump power of 520 mW. The spectral center of the output pulse is 1064 nm, with typical steep edge characteristics, indicating that it is an all-normal dispersion dissipative soliton (Figure S12b, Supporting Information). The 58.8 MHz fundamental mode-locked pulse trains were demonstrated in Figure S12c (Supporting Information), corresponding to the total cavity length. The width of the autocorrelation trace was ≈45 ps and the periodic modulated trace is one of the typical characteristics of bound soliton (Figure S12d, Supporting Information). The maximum average output power is about 11.3 mW, corresponding to the single pulse energy of about ≈192 pJ, which is limited by the output power of the pump laser diode. Commercially available dispersion-compensating fibers in the 1060 nm band are scarce, so most fiber lasers in this band operate as dissipative solitons in the full positive dispersion band, resulting in output pulse widths in the region of one hundred picoseconds,[21] except for the regulation of intracavity dispersion through the introduction of space grating pairs in the fiber ring cavity.[22]

2. Conclusion

We successfully demonstrated a two-step method for growing CNTs directly onto optical fibers to fabricate a new functional fiber, i.e., CNT-PCF. The homogenous and high-quality CNTs with narrow diameter distributions on the inner hole walls of the PCF were obtained by adjusting the concentration and types of

catalyst precursors in the low-pressure CVD method. The CNT-PCF exhibited nonlinear optical application potentials in both THG and ultrafast fiber lasers, taking advantage of the superior nonlinear susceptibility of CNT in both real and imaginary parts. Specifically, THG could be enhanced by ≈15 times compared with flat samples, even surpassing that of graphene fibers. Ultrafast dual-wavelength all-fiber laser was also demonstrated with ≈800 fs pulse width and ≈71 MHz repetition rate. Further, by using CNT-PCF with different CNT diameters, ultrafast fiber lasers covering all the major wavelengths between 1 and 2 μm or even below 1 μm could be realized. Our results can enable the large-scale applications of CNTs based on this new functional fiber.

3. Experimental Section

Injection of Catalyst Precursors into Optical Fibers: Catalyst precursors (Fe or W) were injected into the fibers of their corresponding saline ethanol solutions at optimized concentrations. To ensure full coverage of CNT growth, the amount of catalyst precursor was adjusted based on the catalytic activity of the corresponding catalyst. Typical concentrations are as follows: $FeCl_3$ at ≈2 mmol L^{-1}, $(NH_4)_6W_7O_{24}$ at ≈2.5 mmol L^{-1}. Then, the as-injected fibers were immediately heated to 200 °C and dried in the air for 2 h before CNT growth.

Syntheses of CNT-Embedded Optical Fibers: The fibers coated with catalyst precursors on the inner wall were transferred into a one-inch quartz tube and placed at the center of a CVD furnace. The furnace chamber was then raised to the optimized growth temperature of ≈820 °C in air and flushed with argon (300 sccm) to create an inert atmosphere. Subsequently, hydrogen was introduced to facilitate the transformation of the catalyst precursors into catalyst nanoparticles. Finally, the carbon sources (ethylene 50 sccm) were introduced, and the entire process was carried out at a pressure of ≈400 Pa for a growth duration of 15–30 min. After the CNT growth, the system was naturally cooled down to room temperature.

Characterization of CNT-Embedded Optical Fibers: Optical photographs were taken using a microscope by focusing on the holes in the fiber. Raman mapping was collected using both the WITec alpha300 system and Jovin Yvon-Horiba LabRam systems, with excitation wavelengths of 488, 514, and 633 nm. SEM images were obtained on a Hitachi S4800 SEM, operated at 1.0 kV.

Harmonic Generation Measurements: The THG of hollow core fiber embedded with CNT film was excited with femtosecond pulses (Coherent laser, ≈150 fs, 250 kHz) generated by a Ti: sapphire oscillator pumping an OPA. An objective (Nikon objective, ×4, NA = 0.1) was used to focus the excited light onto the CNT-HCF. The generated THG signal was collected by a Princeton SP2500 spectrometer after being filtered by a 650 nm short-pass filter.

Saturable Absorption Measurements: Femtosecond pulses (Coherent Mira-OPO-X, 1064 nm, ≈150 fs, 76 MHz) generated by a Ti: sapphire oscillator (Coherent, Mira-HP) were coupled to a 90:10 coupler for measuring the saturable absorption characteristics of CNT-HC-1060. A fiber laser (Origami, ≈150 fs, ≈100 MHz) generates ultrafast light centered at 1550 nm connected via a flange to a 90:10 coupler, of which 10% is used for real-time power monitoring and the remaining 90% for measuring the saturable absorption characteristics of the CNT-HC-1550.

Characterization of All-Fiber Mode-Locked Laser at Dual Wavelengths: For the 1561 nm fiber laser, a 980 nm diode laser with a maximum output power of 600 mW was coupled into the ring cavity of the fiber laser via a wavelength division multiplexer (980 nm/1550 nm) and then pumps the erbium-doped gain fiber (60 cm, Er110 4–125, LIEKKI). The near-zero total group velocity dispersion (0.001 ps^2) of the 1550 nm ring cavity was designed for dispersion management soliton generation. The isolator in the ring cavity is designed to prevent backwards transmitted light in the cavity from adversely affecting the fiber laser system. The CNT-PCF (3 cm, NKT, HC-1550) was integrated into the ring cavity by a homemade two-axis alignment system. The polarization controller optimizes spectral and pulse width results by fine-tuning intracavity dispersion and nonlinearity. For the 1064 nm fiber laser, the pump source follows the 980 nm diode laser, the operating band of the wavelength division multiplexer was changed to 980 nm/1064 nm, the gain medium was chosen to be a ytterbium-doped fiber (≈65 cm, YDF, LIEKKI Yb1200-4/125), the operating band of both the ISO and the output coupler was chosen to be 1064 nm and all devices were connected via SMF (HI-1064, Corning). The normal net cavity dispersion (0.0782 ps^2) of the ring cavity was designed for dissipative solitons generation. The ring cavity is not equipped with filter pieces and there is a certain filtering effect with the combination of PCF, isolator, and polarization controller. The spectra were measured by a Fourier transform infrared spectrometer (OSA205C, Thorlabs), the pulse width by autocorrelation (Pulsecheck USB 50, APE), and the repetition frequency by an oscilloscope (DS6104, Rigol) and photodetector (DET08CFC/M, Thorlabs).

Supporting Information

Supporting Information is available from the Wiley Online Library or from the author.

Acknowledgements

This work was financially supported by the Ministry of Science and Technology of China (2016YFA0200100 and 2018YFA0703502), the National Natural Science Foundation of China (Grant Nos. 52021006, T2188101, 52025023, 51720105003, 21790052, 21974004, 52102032, 92256202, U22A20399, 22221001, 22073038), the Strategic Priority Research Program of CAS (XDB36030100), the Beijing National Laboratory for Molecular Sciences (BNLMS-CXTD-202001), the 111 project 2.0 (BP1221004), and the Fundamental Research Funds for the Central Universities (lzujbky-2022-kb0).

Conflict of Interest

The authors declare no conflict of interest.

Author Contributions

Q.X., J.X..J.Z., and K.H.L. conceived the experiments and supervised the project. Q.X. conceived the growth experiments. J.X. and K.F.L. performed the optical experiments and fiber laser setup. Q.X. conducted the SEM, AFM, and Raman characterizations. L.Q., G.J.Y., and H.L.Z. suggested the characterizations and analysis. All the authors discussed the results and wrote the manuscript.

Data Availability Statement

The data that support the findings of this study are available in the supplementary material of this article.

Keywords

carbon nanotube, chemical vapor deposition, diameter control, mode-locked fiber laser, photonic crystal fiber, third-harmonic generation

Received: April 2, 2023
Revised: May 15, 2023
Published online: July 18, 2023

[1] a) S. Yamashita, A. Martinez, B. Xu, *Opt. Fiber Technol.* **2014**, *20*, 702; b) L. Qian, Y. Xie, S. Zhang, J. Zhang, *Matter* **2020**, *3*, 664; c) V. S. Abhisha, R. Stephen, in *Handbook of Carbon Nanotubes* (Eds: J. Abraham, S. Thomas, N. Kalarikkal), Springer International Publishing, Cham **2022**, p. 131.

[2] a) A. Martinez, Z. Sun, *Nat. Photonics* **2013**, *7*, 842; b) S. Yamashita, *J. Lightwave Technol.* **2012**, *30*, 427; c) Y. Tan, *Chemosensors* **2018**, *6*, 55.

[3] a) K. F. Mak, J. C. Travers, P. Holzer, N. Y. Joly, P. S. Russell, *Opt. Express* **2013**, *21*, 10942; b) Y.-W. Song, S. Yamashita, C. S. Goh, S. Y. Set, *Opt. Lett.* **2006**, *32*, 148.

[4] a) Y.-W. Song, K. Morimune, S. Y. Set, S. Yamashita, *Appl. Phys. Lett.* **2007**, *90*, 021101; b) K. Kieu, M. Mansuripur, *Opt. Lett.* **2007**, *32*, 2242; c) K. Kashiwagi, S. Yamashita, *Opt. Express* **2009**, *17*, 18364.

[5] S. Y. Choi, F. Rotermund, H. Jung, K. Oh, D.-I. Yeom, *Opt. Express* **2009**, *17*, 21788.

[6] K. T. Kim, D. S. Yoon, G.-i. Kwoen, *Opt. Commun.* **2004**, *230*, 137.

[7] A. J. Fielding, K. Edinger, C. C. Davis, *J. Lightwave Technol.* **1999**, *17*, 1649.

[8] a) C. Markos, J. C. Travers, A. Abdolvand, B. J. Eggleton, O. Bang, *Rev. Mod. Phys.* **2017**, *89*, 045003; b) D. Cotter, R. J. Manning, K. J. Blow, A. D. Ellis, A. E. Kelly, D. Nesset, I. D. Phillips, A. J. Poustie, D. C. Rogers, *Science* **1999**, *286*, 1523; c) K. Chen, X. Zhou, X. Cheng, R. Qiao, Y. Cheng, C. Liu, Y. Xie, W. Yu, F. Yao, Z. Sun, F. Wang, K. Liu, Z. Liu, *Nat. Photonics* **2019**, *13*, 754; d) Y. Zuo, W. Yu, C. Liu, X. Cheng, R. Qiao, J. Liang, X. Zhou, J. Wang, M. Wu, Y. Zhao, P. Gao, S. Wu, Z. Sun, K. Liu, X. Bai, Z. Liu, *Nat. Nanotechnol.* **2020**, *15*, 987.

[9] a) P. Russell, *Science* **2003**, *299*, 358; b) J. C. Knight, *Nature* **2003**, *424*, 847.

[10] a) Y. Cheng, W. Yu, J. Xie, R. Wang, G. Cui, X. Cheng, M. Li, K. Wang, J. Li, Z. Sun, K. Chen, K. Liu, Z. Liu, *ACS Photonics* **2022**, *9*, 961; b) G. Q. Ngo, A. George, R. T. K. Schock, A. Tuniz, E. Najafidehaghani, Z. Gan, N. C. Geib, T. Bucher, H. Knopf, S. Saravi, C. Neumann, T. Luhder, E. P. Schartner, S. C. Warren-Smith, H. Ebendorff-Heidepriem, T. Pertsch, M. A. Schmidt, A. Turchanin, F. Eilenberger, *Adv. Mater.* **2020**, *32*, 2003826.

[11] a) X. Li, H. Zhu, *J. Materiomics* **2015**, *1*, 33; b) A. K. Geim, *Science* **2009**, *324*, 1530.

[12] a) S. Zhang, L. Kang, X. Wang, L. Tong, L. Yang, Z. Wang, K. Qi, S. Deng, Q. Li, X. Bai, F. Ding, J. Zhang, *Nature* **2017**, *543*, 234; b) S. Zhang, X. Wang, F. Yao, M. He, D. Lin, H. Ma, Y. Sun, Q. Zhao, K. Liu, F. Ding, J. Zhang, *Chem* **2019**, *5*, 1182.

[13] a) Y. Xie, L. Qian, D. Lin, Y. Yu, S. Wang, J. Zhang, *Angew. Chem., Int. Ed.* **2021**, *60*, 9330; b) Y. Hu, L. Kang, Q. Zhao, H. Zhong, S. Zhang, L. Yang, Z. Wang, J. Lin, Q. Li, Z. Zhang, L. Peng, Z. Liu, J. Zhang, *Nat. Commun.* **2015**, *6*, 6099.

[14] a) Q. Zhao, J. Zhang, *Small* **2014**, *10*, 4586; b) A. Jorio, R. Saito, J. H. Hafner, C. M. Lieber, M. Hunter, T. McClure, G. Dresselhaus, M. S. Dresselhaus, *Phys. Rev. Lett.* **2001**, *86*, 1118; c) Y. Yao, Q. Li, J. Zhang, R. Liu, L. Jiao, Y. T. Zhu, Z. Liu, *Nat. Mater.* **2007**, *6*, 283.

[15] L. Qian, Q. Shao, Y. Yu, W. Liu, S. Wang, E. Gao, J. Zhang, *Adv. Funct. Mater.* **2021**, *32*, 2106643.

[16] V. A. Margulis, T. A. Sizikova, *Phys. B* **1998**, *245*, 173.

[17] B. Jiang, Z. Hao, Y. Ji, Y. Hou, R. Yi, D. Mao, X. Gan, J. Zhao, *Light: Sci. Appl.* **2020**, *9*, 63.

[18] a) P. Avouris, M. Freitag, V. Perebeinos, *Nat. Photonics* **2008**, *2*, 341; b) K. Y. Lau, X. Liu, J. Qiu, *Adv. Photonics Res.* **2022**, *3*, 2200023.

[19] S. Xu, F. Q. Wang, C. H. Zhu, Y. F. Meng, Y. J. Liu, W. Q. Liu, J. Y. Tang, K. H. Liu, G. H. Hu, R. C. T. Howe, T. Hasan, R. Zhang, Y. Shi, Y. B. Xu, *Nanoscale* **2016**, *8*, 9304.

[20] a) J. S. Lauret, C. Voisin, G. Cassabois, C. Delalande, P. Roussignol, O. Jost, L. Capes, *Phys. Rev. Lett.* **2003**, *90*, 057404; b) C. Manzoni, A. Gambetta, E. Menna, M. Meneghetti, G. Lanzani, G. Cerullo, *Phys. Rev. Lett.* **2005**, *94*, 207401.

[21] Y. Z. Pan, J. G. Miao, W. J. Liu, X. J. Huang, Y. B. Wang, *Laser Phys. Lett.* **2014**, *11*, 095105.

[22] L. Hou, H. Guo, Y. Wang, J. Sun, Q. Lin, Y. Bai, J. Bai, *Opt. Express* **2018**, *26*, 9063.